Quantitative lifetime unmixing of multiexponentially decaying fluorophores using single-frequency fluorescence lifetime imaging microscopy

Kremers, G.J.; van Munster, E.B.; Goedhart, J.; Gadella, Th.W.J.

DOI
10.1529/biophysj.107.125229

Publication date
2008

Published in
Biophysical Journal

Quantitative Lifetime Unmixing of Multiexponentially Decaying Fluorophores Using Single-Frequency Fluorescence Lifetime Imaging Microscopy

Gert-Jan Kremers, Erik B. van Munster, Joachim Goedhart, and Theodorus W. J. Gadella Jr.
Section Molecular Cytology and Centre for Advanced Microscopy, Swammerdam Institute for Life Sciences, University of Amsterdam, Kruislaan 316, NL-1098 SM, Amsterdam, The Netherlands

ABSTRACT Fluorescence lifetime imaging microscopy (FLIM) is a quantitative microscopy technique for imaging nanosecond decay times of fluorophores. In the case of frequency-domain FLIM, several methods have been described to resolve the relative abundance of two fluorescent species with different fluorescence decay times. Thus far, single-frequency FLIM methods generally have been limited to quantifying two species with monoexponential decay. However, multiexponential decays are the norm rather than the exception, especially for fluorescent proteins and biological samples. Here, we describe a novel method for determining the fractional contribution in each pixel of an image of a sample containing two (multiexponentially) decaying species using single-frequency FLIM. We demonstrate that this technique allows the unmixing of binary mixtures of two spectrally identical cyan or green fluorescent proteins, each with multiexponential decay. Furthermore, because of their spectral identity, quantitative images of the relative molecular abundance of these fluorescent proteins can be generated that are independent of the microscope light path. The method is rigorously tested using samples of known composition and applied to live cell microscopy using cells expressing multiple (multiexponentially decaying) fluorescent proteins.

INTRODUCTION

Fluorescence lifetime imaging microscopy (FLIM) provides spatially resolved information of the fluorescence lifetime of a fluorophore. Because the fluorescence lifetime (τ) of a fluorophore can be influenced by its direct molecular environment, FLIM has been applied in cell biology for measuring physiological parameters in the cell, for example, cellular pH, ion concentrations, and membrane potential (1–3). At present, the major application of FLIM is the measurement of protein-protein interactions by means of fluorescence resonance energy transfer (FRET) using fluorescently labeled proteins (4–7).

Besides measuring changes in lifetime, FLIM can also be used to quantitatively image the spatial (and fractional) distribution of two (noninteracting) fluorescent probes with different lifetimes. This provides the opportunity to image the spatial distribution of two different probes (8) or the abundance of two different states of a single fluorescent probe, for example, the fraction of protein undergoing energy transfer in a FRET experiment (9).

Several methods have been developed that employ FLIM for the quantification of the fractional probe distribution of binary mixtures. In time-domain FLIM data, the composition of mixtures of two fluorophores can be resolved by fitting the fluorescence decay to a biexponential function if both fluorophores exhibit a monoexponential lifetime (10). The problem becomes more complicated when the fluorophores exhibit multiexponential fluorescence decay. Resolving the composition of a sample having three or more exponential components is time consuming and requires high data quality. The most advanced time-correlated single-photon counting systems are able to resolve more than three exponential components; however, lifetime imaging of biological samples hardly ever provides the data quality required for such resolution.

In frequency-domain FLIM, resolving the composition of mixed fluorophores is an important issue as well. In the case of a mixed sample of two (or even three) fluorescent species with monoexponential and known lifetimes, the fractional contribution of each species can be quantitatively resolved using the dispersion relationships in Eqs. A4 and A5 (8). However, when the lifetimes of the components in a mixture are not known or the mixture contains fluorophores with multiexponential fluorescence decay, quantification of the fractional contribution is not straightforward or is even impossible. Multifrequency FLIM (11), where the specimen is sampled at multiple modulation frequencies, can in principle solve such a complex problem, but the long exposure time of such experiments excludes many biological applications. Alternative approaches have been developed, including global analysis of data sets and the graphical representation of FLIM data in a polar or phasor plot. Global analysis has the advantage that a priori knowledge of the lifetime of each species is not required (12,13). Global analysis estimates the lifetimes of the fluorophores based on the distribution of lifetime values in a data set, thereby extracting a larger

Submitted November 20, 2007, and accepted for publication February 21, 2008.

Address reprint requests to Gert-Jan Kremers, E-mail: gertjan.kremers@vanderbilt.edu.

Gert-Jan Kremers's present address is Dept. of Molecular Physiology and Biophysics, Vanderbilt University Medical Center, 702 Light Hall, Nashville, TN 37232.

Editor: G. Barisas.

0006-3495/08/07/378/12 $2.00

doi: 10.1529/biophysj.107.125229

amount of information from the experimental data. A limitation of global analysis is that it can be applied only to fluorophores with monoexponential fluorescence decay.

The actual lifetime distribution obtained from frequency-domain FLIM data can be difficult to interpret due to the nonlinear relation between the phase and modulation lifetimes. It is possible to transform the measured phase and modulation into a coordinate system where they become linear functions of the fractional composition of the species (14–16). Such graphical representation is called a polar or phasor plot. Using the phasor plot representation, the problem of resolving the composition of a mixture is reduced to a linear fitting procedure. Mixtures containing multiexponentially decaying fluorophores can be resolved as well, if the phase and modulation of each fluorophore are known. A phasor plot can be used to analyze both frequency-domain and time-domain FLIM data (16).

Single-frequency FLIM lifetime unmixing of probes with multiexponential fluorescence decay

Until now, most methods for resolving the composition of mixed fluorophores have generally been limited to fluorescent species with monoexponential fluorescence decays. Since many fluorophores, and almost all fluorescent proteins, display a more complex multiexponential decay, methods to quantify the composition of mixed samples containing fluorophores with multiexponential lifetimes are of great interest. The challenge is to still generate information on the relative abundance of the individual species from such FLIM data. However, in all cases a simplification of the situation or an assumption about the sample and additional mathematics are required to face this challenge. Here, we present a method for quantitative lifetime unmixing based on single-frequency FLIM measurements that can deal with dual-component systems of fluorophores displaying multiexponential fluorescence decay.

We have developed a method using the phase shift and demodulation of fluorescence, rather than looking for the actual lifetime distributions of each component. For any fluorophore, τ_φ and τ_m are exact representations of the phase shift and demodulation induced by the fluorophore at a given modulation frequency. Assuming τ_φ and τ_m for each of the two fluorophores are known, we have formulated a mathematical solution to unmix the fractional contribution of the two fluorophores based on the apparent τ_φ and τ_m of the mixture using single-frequency FLIM. Therefore, we call this method lifetime unmixing of single-frequency FLIM data.

Theory

To be able to determine the fractional contribution of two fluorophores in a mixture by single-frequency FLIM lifetime unmixing, we have analytically derived the relation between τ_φ and τ_m of the mixture and the fractional contribution of each probe. For a general theoretical description of phase fluorometry from which the equations are derived, the reader is referred to Weber (17) and the appendix. In frequency-domain FLIM the excitation light is intensity modulated. As a result, the emitted fluorescence $F_i(t)$ is modulated at the same high frequency, but due to the noninstant fluorescence decay the fluorescence will be phase-shifted ($\Delta\varphi_i$) and demodulated ($M_{F,i}$) according to

$$F_i(t) = F_{0,i}(1 + M_{F,i}\sin(\omega t - \Delta\varphi_i)). \tag{1}$$

The subscript i refers to the ith species in the sample, $F_{0,i}$ is the average (steady-state) fluorescence intensity, and ω is the angular frequency of modulation.

For a sample containing two fluorescent species, the total emitted fluorescence will be the sum of the fluorescence emitted by each fluorophore:

$$F(t) = F_1(t) + F_2(t) = F_{0,1} + F_{0,2} + F_{0,1}M_{F,1}\sin(\omega t - \Delta\varphi_1) + F_{0,2}M_{F,2}\sin(\omega t - \Delta\varphi_2), \tag{2a}$$

which can also be formulated as

$$F(t) = F_{0,1} + F_{0,2} + \sin\omega t(F_{0,1}M_{F,1}\cos\Delta\varphi_1 + F_{0,2}M_{F,2}\cos\Delta\varphi_2) - \cos\omega t(F_{0,1}M_{F,1}\sin\Delta\varphi_1 + F_{0,2}M_{F,2}\sin\Delta\varphi_2). \tag{2b}$$

Eq. 2b can be written in a form similar to Eq. A1b:

$$F(t) = L + G\sin\omega t - S\cos\omega t = L + \sqrt{S^2 + G^2}\sin\left(\omega t - \tan^{-1}\left(\frac{S}{G}\right)\right), \tag{3a}$$

where

$$\begin{cases} L = F_{0,1} + F_{0,2} \\ S = F_{0,1}M_{F,1}\sin\Delta\varphi_1 + F_{0,2}M_{F,2}\sin\Delta\varphi_2 \\ G = F_{0,1}M_{F,1}\cos\Delta\varphi_1 + F_{0,2}M_{F,2}\cos\Delta\varphi_2 \end{cases}. \tag{3b}$$

By comparing Eq. 3 to Eqs. A1b and A2, it follows that the modulation of the fluorescence of the mixture can be described as a sinusoid with apparent phase shift ($\Delta\varphi'$) and modulation (M′):

$$\Delta\varphi' = \tan^{-1}\left(\frac{S}{G}\right) \tag{4a}$$

$$\text{and} \quad M' = \frac{\sqrt{S^2 + G^2}}{L}. \tag{4b}$$

Hence it follows that the apparent phase and modulation lifetimes are described as

$$\tau'_\varphi \equiv \frac{1}{\omega}\frac{S}{G} \tag{5a}$$

$$\text{and} \quad \tau'_m \equiv \frac{1}{\omega}\sqrt{\frac{L^2}{S^2 + G^2} - 1}. \tag{5b}$$

If the lifetimes $\tau_{\varphi,j}$ and $\tau_{m,j}$ of both fluorescent species are known, this information can be used to calculate $\Delta\varphi_j$ and M_j for both probes using Eq. A2. In this case, the only unknown

parameters are the contribution of each probe ($F_{0,j}$) to the steady-state fluorescence. The fractional contribution (α) of the $F_{0,1}$ fluorescent species can be defined as

$$\alpha \equiv \frac{F_{0,1}}{F_{0,1}+F_{0,2}}. \tag{6}$$

Substitution of α for $F_{0,1}$ and $F_{0,2}$ in Eq. 3 enables us to define α as a function of τ'_φ and τ'_m, respectively, as follows. By combining Eqs. 3, 5a, and 6, we can write the apparent τ'_φ of the binary mixture as a function of α:

$$\tau'_\phi = \frac{1}{\omega}\frac{S}{G} = \frac{\alpha M_{F,1}\sin\Delta\varphi_1 + (1-\alpha)M_{F,2}\sin\Delta\varphi_2}{\omega(\alpha M_{F,1}\cos\Delta\varphi_1 + (1-\alpha)M_{F,2}\cos\Delta\varphi_2)} \tag{7}$$

from which we can isolate α:

$$\alpha = \frac{\omega\tau'_\varphi M_{F,2}\cos\Delta\varphi_2 - M_{F,2}\sin\Delta\varphi_2}{M_{F,1}\sin\Delta\varphi_1 - M_{F,2}\sin\Delta\varphi_2 - \omega\tau'_\varphi M_{F,1}\cos\Delta\varphi_1 + \omega\tau'_\varphi M_{F,2}\cos\Delta\varphi_2}, \tag{8}$$

which can be rewritten in the form

$$\alpha = \frac{A - B\tau'_\varphi}{C - D\tau'_\varphi};\ \begin{cases} A = M_{F,2}\sin\Delta\varphi_2 \\ B = \omega M_{F,2}\cos\Delta\varphi_2 \\ C = M_{F,2}\sin\Delta\varphi_2 - M_{F,1}\sin\Delta\varphi_1 \\ D = \omega(M_{F,2}\cos\Delta\varphi_2 - M_{F,1}\cos\Delta\varphi_1) \end{cases};\ \begin{cases} \sin\Delta\varphi_j \equiv \dfrac{\omega\tau_{\varphi_j}}{\sqrt{1+\omega^2\tau_{\varphi_j}^2}} \\ \cos\Delta\varphi_j \equiv \dfrac{1}{\sqrt{1+\omega^2\tau_{\varphi_j}^2}}, \\ M_{F,j} = \dfrac{M_E}{\sqrt{1+\omega^2\tau_{m_j}^2}} \end{cases} \tag{9}$$

where the constants A, B, C, and D are all defined by the phase shift (or $\tau_{\varphi,j}$) and demodulation (or $\tau_{m,j}$) of the isolated fluorophores.

Alternatively, by combining Eqs. 3, 5b, and 6 we can write the apparent τ'_m of the binary mixture as a function of α as follows:

$$\tau'_m = \frac{1}{\omega}\sqrt{\frac{L^2}{S^2+G^2}-1} = \frac{1}{\omega}\sqrt{\frac{1}{(\alpha M_{F,1}\sin\Delta\varphi_1 + (1-\alpha)M_{F,2}\sin\Delta\varphi_2)^2 + (\alpha M_{F,1}\cos\Delta\varphi_1 + (1-\alpha)M_{F,2}\cos\Delta\varphi_2)^2} - 1} \tag{10}$$

from which we can isolate α:

$$P\alpha^2 + Q\alpha + R = 0, \tag{11a}$$

$$\text{and}\quad \alpha = \frac{-Q + \sqrt{Q^2 - 4PR}}{2P}, \tag{11b}$$

where

$$\begin{cases} P = M_{F,1}^2 + M_{F,2}^2 - 2M_{F,1}M_{F,2}(\sin\Delta\varphi_1\sin\Delta\varphi_2 + \cos\Delta\varphi_1\cos\Delta\varphi_2) \\ Q = -2M_{F,2}^2 + 2M_{F,1}M_{F,2}(\sin\Delta\varphi_1\sin\Delta\varphi_2 + \cos\Delta\varphi_1\cos\Delta\varphi_2) \\ R = M_{F,2}^2 - \dfrac{M_E^2}{1+\omega^2\tau'^2_m} \end{cases}. \tag{11c}$$

We have now derived two equations from which experimental FLIM data, i.e., τ'_φ and τ'_m of the mixture and $\Delta\varphi$ and M of the pure (multiexponential) components, can be related to the fractional composition of a binary mixture. Eqs. 9 and 11 allow independent estimations, based on τ'_φ and τ'_m, respectively. Ideally, both equations should yield the same value for α.

Application of lifetime unmixing to spectrally identical fluorescent proteins

In this work, we apply single-frequency lifetime unmixing to two pairs of fluorescent proteins (in general, visible fluorescent proteins or VFPs). Recently, we reported on pairs of cyan and green fluorescent proteins (CFPs and GFPs, respectively) with markedly different fluorescence lifetimes (18,19) Table 1. SCFP3A and SCFP1 are CFPs with, respectively, long and short fluorescence lifetimes. Both CFPs have identical excitation and emission spectra (Fig. 1 *A*). Analogously, SGFP2 and SGFP2(T65G) are GFP variants with long and short fluorescence lifetimes, respectively. SGFP2(T65G) and SGFP2 have identical emission spectra but different excitation spectra (Fig. 1 *B*).

The advantage of fluorescent proteins with different lifetimes but identical emission spectra is that these probes can

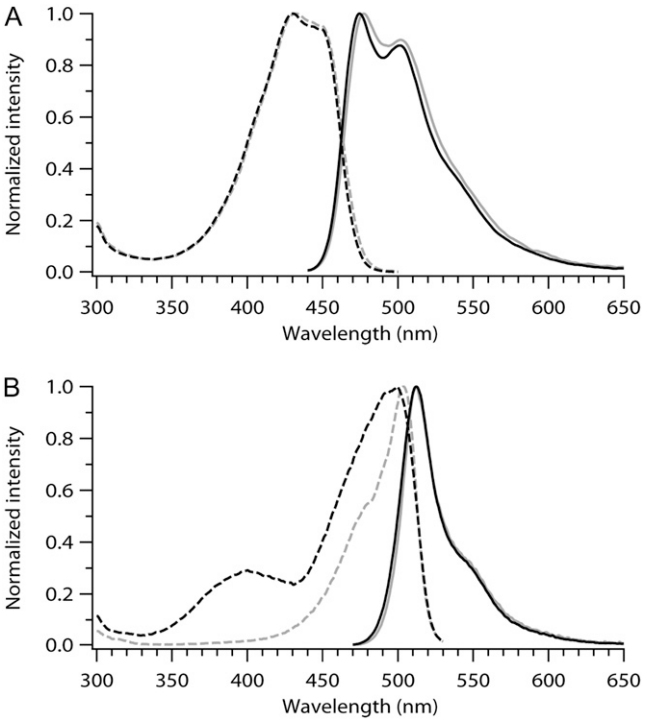

FIGURE 1 Excitation (*dotted lines*) and emission spectra (*solid lines*) of fluorescent proteins. (*A*) Spectra of SCFP1 (*gray*) and SCFP3A (*black*). (*B*) Spectra of SGFP2(T65G) (*gray*) and SGFP2 (*black*).

be detected through a single narrow bandpass filter, thereby claiming only a small part of the visible spectrum. The remaining part of the spectrum can then be used for imaging additional fluorescent probes. Furthermore, the application of fluorescent proteins with identical emission spectra has the advantage that fractional contributions based on fluorescence can be converted to molar ratios if the relative intrinsic brightness of the fluorescent proteins (product of molar extinction coefficient and *QY*) is known.

MATERIALS AND METHODS

Preparation of purified protein samples

Fluorescent proteins were purified as described before (19). VFP stock solutions with optical density ≈0.05 were prepared in phosphate buffer saline, pH 7.4, and adjusted to equal fluorescence intensity in a PTI QuantaMaster 2000-4 fluorescence spectrofluorometer (Photon Technology International, Lawrenceville, NJ). A series of mixtures with defined composition was prepared from these stock solutions, and 90 μl of each mixture was used to fill wells of a flat bottom 96-wells plate (Greiner Bio-One, Frickenhausen, Germany) for lifetime measurements.

Construction of VFP expression vectors

Construction of mammalian expression vectors encoding SCFP1-NLS, SCFP3A-NES, SGFP2, SGFP2(T65G), and SYFP2 have been described previously (18,19). SCFP1-NLS is targeted to the nucleus by the nuclear localization sequence (NLS). SCFP3A-NES is excluded from the nucleus because of a nuclear export sequence (NES). SGFP2-NES-PHgrp1 was constructed by ligating the pleckstrin homology (PH) domain of GRP1 (20) to the C-terminus of SGFP2. A NES was used as a linker between SGFP2 and PHgrp1. mCherry-SYFP2 consisted of a fusion of the red fluorescent protein (RFP) mCherry (21) to the N-terminus of the yellow fluorescent protein (YFP) SYFP2 separated by a 17 amino acid flexible linker (SGLRSRA-QASNSAVDGT).

Sample preparation for live cell imaging

HeLa or Swiss 3T3 cells were grown on glass coverslips (Ø 24 mm) and transfected with 0.2–0.4 μg plasmid DNA, using 1.5 μl Lipofectamine2000 (Invitrogen, Carlsbad, CA). To obtain mixed populations of cells expressing different DNA constructs, cells were trypsinized and pooled 8 h after transfection. Cells were used for microscopy 16–24 h after transfection. Cells were imaged in extracellular-like buffer (140 mM NaCl, 5 mM KCl, 1 mM $CaCl_2$, 1 mM $MgCl_2$, 10 mM glucose, and 20 mM Hepes, pH 7.4). Swiss 3T3 cells were serum starved 4 h before imaging. Phosphatidylinositol(3,4,5) trisphosphate (PtdIns(3,4,5)P_3) production was triggered by stimulation with 10 ng/ml platelet-derived growth factor (PDGF-BB; Sigma-Aldrich, St. Louis, MO).

FLIM measurements

For frequency-domain wide-field FLIM measurements, the FLIM setup as described by van Munster et al. (22) was used. For imaging CFP and GFP, a helium-cadmium laser (442 nm 125 mW) or argon-ion laser (488 nm 150 mW) (Melles-Griot, Carlsbad, CA), a 455DCLP or Q495LP dichroic mirror, and a D480/40 or HQ515/30 bandpass emission filter (Chroma Technology, Rockingham, VT) were used, respectively. The frequency of modulation was 75 MHz. For each lifetime measurement the reference phase and modulation were obtained, using a reference filter cube reflecting 0.1% of the excitation laser light directly onto the detector. The FLIM setup was calibrated based on the fluorescence lifetime of erythrosin B, assuming a monoexponential lifetime of 86 ps (23). FLIM stacks of 15 phase images were acquired with an exposure time of 50–500 ms per image, depending on the brightness of the samples, using a Zeiss plan Neofluar 40× 1.3 NA, oil immersion objective (Zeiss, Jena, Germany). To minimize artifacts due to photobleaching, a permutated recording sequence was used (24). Software for control, acquisition, processing, and analysis of the data were written in C++, using

TABLE 1 Properties of fluorescent protein variants

	ε (λ_{ex})*	QY (λ_{em})†	$\varepsilon \times QY$‡	pK_a	τ_φ (ns)	τ_m (ns)
SCFP1	29 (434)	0.24 (477)	1	<3.5	1.42 ± 0.02	1.80 ± 0.01
SCFP3A	30 (434)	0.56 (474)	2.4	<4.5	2.76 ± 0.03	3.30 ± 0.01
SGFP2(T65G)	90 (501)	0.35 (512)	1	6.7	1.52 ± 0.03	1.64 ± 0.02
SGFP2	46 (495)	0.70 (512)	1.3	5.9	2.93 ± 0.05	2.94 ± 0.03

*Extinction coefficient (10^3 $M^{-1}cm^{-1}$) with absorbance maximum (nm) between brackets.
†Quantum yield with emission maximum (nm) between brackets.
‡Intrinsic brightness of purified protein relative to SCFP1 and SGFP2(T65G), respectively. The intrinsic brightness of the GFP variants is corrected for the excitation efficiency at 488 nm. Lifetimes are the mean ± SD of six measurements.

MATLAB 6.1 (The MathWorks, Natick, MA) and the image processing library DIPlib (Pattern Recognition Group, TU Delft, the Netherlands, http://www.ph.tn.tudelft.nl/DIPlib/).

Global analysis of FLIM data

The FLIM image stacks recorded for the SGFP2(T65G)/SGFP2 mixtures were analyzed simultaneously by an optimized global analysis algorithm for single-frequency FLIM data (12). The global analysis is based on the assumption of the presence of two spatially invariant (monoexponential) fluorescence lifetimes (τ_1 and τ_2) with a spatially variable fractional contribution. We used software described in Verveer and Bastiaens (12) which minimizes the following χ^2 using an iterative Levenberg-Marquardt algorithm with numerical derivatives:

$$\chi^2(\tau_1,\tau_2)=\sum_i \frac{((\omega^2\tau_1\tau_2-1)B_i-\omega(\tau_1+\tau_2)A_i+1)^2}{\omega^2(\tau_1+\tau_2)^2\sigma_{A,i}^2+(\omega^2\tau_1\tau_2-1)^2\sigma_{B,i}^2} \quad (12)$$

with $A_i = M_i' \sin(\Delta\varphi_i')$ and $A_i = M_i' \cos(\Delta\varphi_i')$.

Here the subscript i denotes an individual pixel measurement, $\Delta\varphi_i'$, M_i' represents the pixel values of the measured phase shift and demodulation as defined in Eq. 4 a,b, and $\sigma_{A,i}, \sigma_{B,i}$ represent the estimated standard deviation in A_i, B_i calculated by error propagation from errors in the measured phase shift and modulation. The two lifetimes τ_1 and τ_2 can then be substituted in an equation (Eq. 10 in Verveer and Bastiaens (12)) to find the spatially variable fractional contribution of the first lifetime component. For the two-component mixtures, all FLIM stacks representing the different mixing ratio's (fractional contributions) were taken together and analyzed simultaneously assuming two invariant (global) lifetime components (τ_1 and τ_2) but different fractional contribution per image.

Multiparameter FLIM measurements

For additional lifetime imaging of SYFP2, an argon-ion laser (514 nm, 150 mW) (Melles-Griot), a 525DCXR dichroic mirror, and a HQ545/30 bandpass emission filter (Chroma Technology) were used. For imaging of mCherry fluorescence, light from a 100 W high pressure mercury lamp passed through a HQ546/10 filter was used for excitation, and fluorescence was detected using a 600DCXR dichroic mirror and HQ630/60 emission filter (Chroma Technology).

The FRET efficiency (E) of the mCherry-SYFP2 tandem fusion was calculated based on the lifetime for SYFP2:

$$E = 1 - \frac{\tau_{DA}}{\tau_D}, \quad (13)$$

where, τ_{DA} is the lifetime of SYFP2 fused to mCherry, and τ_D is the lifetime of unfused SYFP2.

RESULTS

Quantitative lifetime unmixing of purified fluorescent protein

The feasibility of quantitative lifetime unmixing with SCFP3A/SCFP1 and SGFP2/SGFP2(T65G) was evaluated by FLIM measurements on mixtures of purified fluorescent proteins with defined composition. Purified fluorescent protein solutions with identical fluorescence intensity were mixed to obtain samples with known fractional composition. For the pure CFP variants, we measured fluorescence lifetimes of τ_φ 1.42 ± 0.02 ns and τ_m 1.80 ± 0.01 ns for SCFP1 and τ_φ 2.76 ± 0.03 ns and τ_m 3.30 ± 0.01 ns for SCFP3A. For all mixtures containing SCFP1 and SCFP3A, intermediate τ_φ' and τ_m' values were observed with $\tau_\varphi' < \tau_m'$. Plotting τ_φ' or τ_m' versus the fractional contribution (α) of SCFP1 in each mixture showed a nonlinear relation between τ_φ' and α; the relation of τ_m' and α appeared more linear (Fig. 2 *A*). Using Eq. 7, τ_φ' as a function of α can be calculated (Fig. 2 *A*, *black line*). The theoretical relation is nonlinear and fits the experimental values perfectly. Similarly, Eq. 10 was used to calculate τ_m' as a function of α (Fig. 2 *A*, *gray line*). The theoretical relation between τ_m' and α seemed almost linear and also fitted the experimental data very well. Nearly perfect linear correlation was observed when the predicted α, based on τ_φ' and τ_m', was plotted versus the true composition (Fig. 2, *B* and *C*; Table 2). These results demonstrate very good agreement between theory and experiment and show that the measured τ_φ' and τ_m' can be used to accurately determine the fractional composition of the samples containing SCFP1 and SCFP3A.

An identical approach was applied to mixtures of SGFP2(T65G) (τ_φ 1.52 ± 0.03 ns; τ_m 1.64 ± 0.02 ns) and SGFP2 (τ_φ 2.93 ± 0.05 ns; τ_m 2.94 ± 0.03 ns). The difference between τ_φ and τ_m for both GFP variants was less than that for SCFP1 and SCFP3A, indicating a more homogeneous fluorescence decay for the GFP variants. The expected apparent lifetimes τ_φ' and τ_m' based on the fractional contribution of SGFP2(T65G) showed similar trends as the CFP variants (Fig. 2 *D*). Plotting the measured τ_φ' and τ_m' versus α indicated that for all mixed samples the measured τ_φ' and τ_m' were slightly higher than the theoretical predictions (Fig. 2 *D*). As a consequence, the estimated fractional contribution of SGFP2(T65G) based on τ_φ' as well as τ_m' was systematically underestimated (Fig. 2, *E* and *F* and Table 2). During the FLIM measurements more pronounced bleaching was observed for SGFP2(T65G) (28%) than for SGFP2 (6%), and the amount of bleaching increased for mixtures containing more SGFP2(T65G) (data not shown). We tested whether photobleaching could explain the underestimation of SGFP2(T65G). Plotting the bleach-corrected values of α (τ_φ') and α (τ_m') versus the true α improved the results of lifetime unmixing, although the changes were within the standard deviation of the measurements (Supplementary Material, Data S1). Photobleaching should be minimized, especially if the two fluorophores exhibit differential photobleaching kinetics, as this can affect the fractional composition of the sample. Together these results indicated that lifetime unmixing enabled the accurate estimation of the fractional composition of binary mixtures of fluorophores, regardless of the complex fluorescence decay in the mixtures.

Comparing lifetime unmixing and global analysis

Previously, global analysis has been used to determine the lifetime components and their fractional contribution in a binary system (12,13). The advantage of global analysis is that a priori knowledge of the lifetime components is not

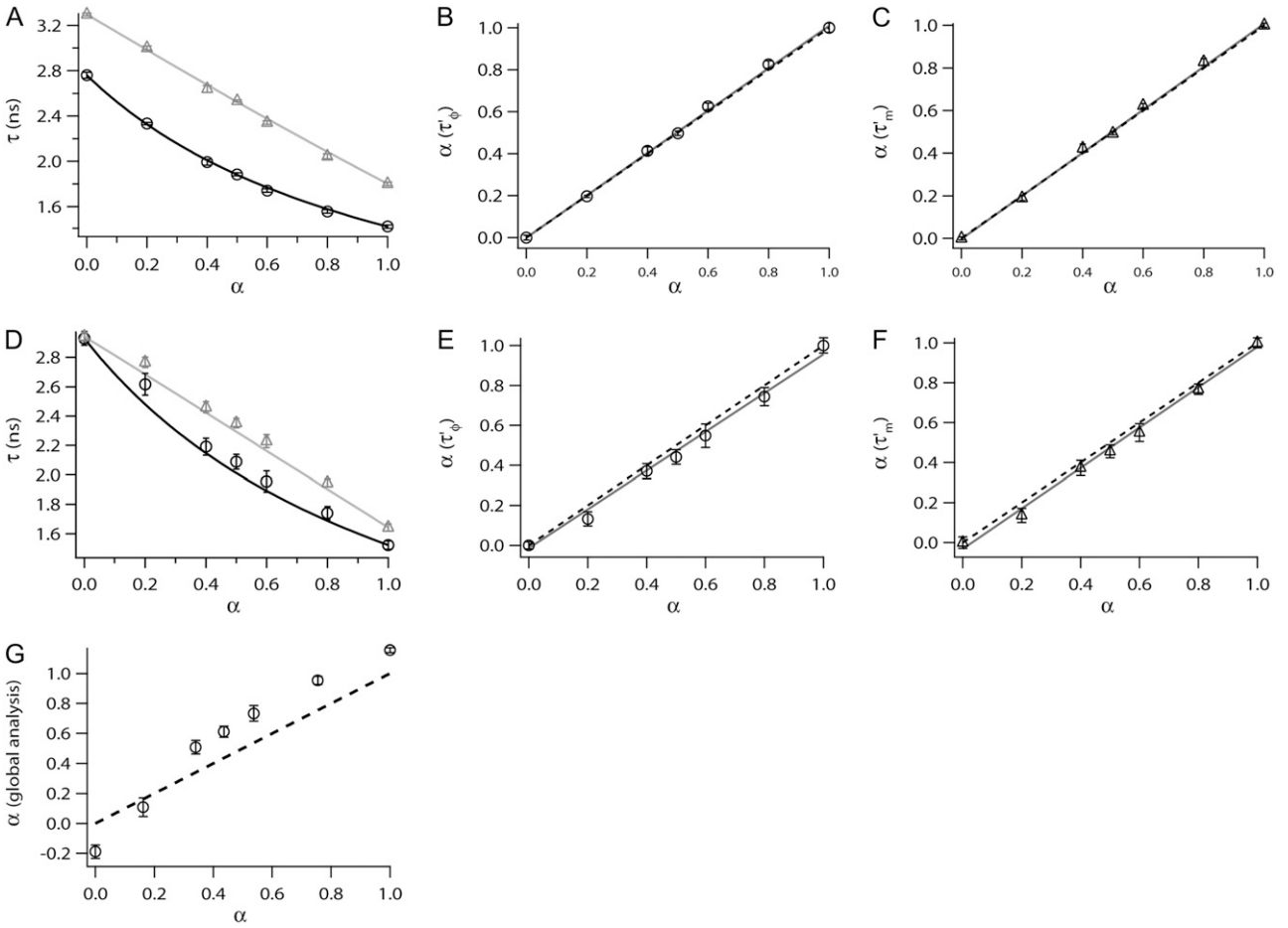

FIGURE 2 Lifetime unmixing of mixtures of purified fluorescent proteins. (*A–C*) Mixtures containing SCFP1 and SCFP3A. (*D–G*) Mixtures containing SGFP2(T65G) and SGFP2. α is the fractional contribution of SCFP1 or SGFP2(T65G) in each sample. (*A* and *D*) Comparison of the measured τ'_φ (○) and τ'_m (△) versus α. The solid lines represent the theoretical relation of τ'_φ (*black*) and τ'_m (*gray*) with α. (*B* and *E*) Correlation between α (τ'_φ) and the true sample composition α. Solid lines are the linear fits, and dotted lines represent α (τ'_φ) = α. (*C* and *F*) Correlation between α (τ'_m) versus the actual sample composition α. Solid lines are the linear fits, and dotted lines represent α (τ'_m) = α. (*G*) Estimation of composition of SGFP2(T65G)/SGFP2 mixtures by global analysis. Dotted line represents α (global analysis) = α. The lifetime values used for unmixing were taken from Table 1. Error bars indicate standard deviation ($n = 6$).

required. Instead the lifetime of each component is estimated from the distribution of lifetimes in the data set. Global analysis is, however, restricted to mixtures of fluorophores with monoexponential lifetime. As the fluorescence decay of SGFP2 and SGFP2(T65G) were closest to monoexponential, we investigated if global analysis could determine the composition of these mixtures. The lifetime for SGFP2 estimated by global analysis was 2.92 ns and similar to the lifetime values measured for τ_φ and τ_m by conventional analysis. The estimated lifetime for SGFP2(T65G) was 1.43 ns and less than τ_φ and τ_m. The reduced lifetime estimation for SGFP2(T65G) was caused by the heterogeneity in its fluorescence decay. Plotting the fractional contribution of SGFP2(T65G) estimated by global analysis versus the true fractional contribution (Fig. 2 *G*) showed large deviations up to 20% and resulted in (unrealistic) values of $\alpha < 0$ and > 1. Thus, global analysis, in contrast to lifetime unmixing, was unable to accurately resolve the composition of the SGFP2(T65G)/SGFP2 mixtures. This was expected, as SGFP2(T65G) does not have a perfect monoexponential lifetime.

TABLE 2 Linear fits lifetime unmixing

	τ	Slope	Intercept	r
SCFP1/SCFP3A	φ	1.01 ± 0.01	0.00 ± 0.01	0.964
	m	1.01 ± 0.01	0.00 ± 0.01	0.962
SGFP2(T65G)/SGFP2	φ	0.97 ± 0.03	−0.01 ± 0.02	0.934
	m	1.01 ± 0.01	−0.03 ± 0.02	0.988

In vivo lifetime unmixing with SCFP1 and SCFP3A

Next, lifetime unmixing was applied to living cells expressing SCFP1-NLS or SCFP3A-NES or coexpressing both fluorescent proteins to segregate the localization of these two

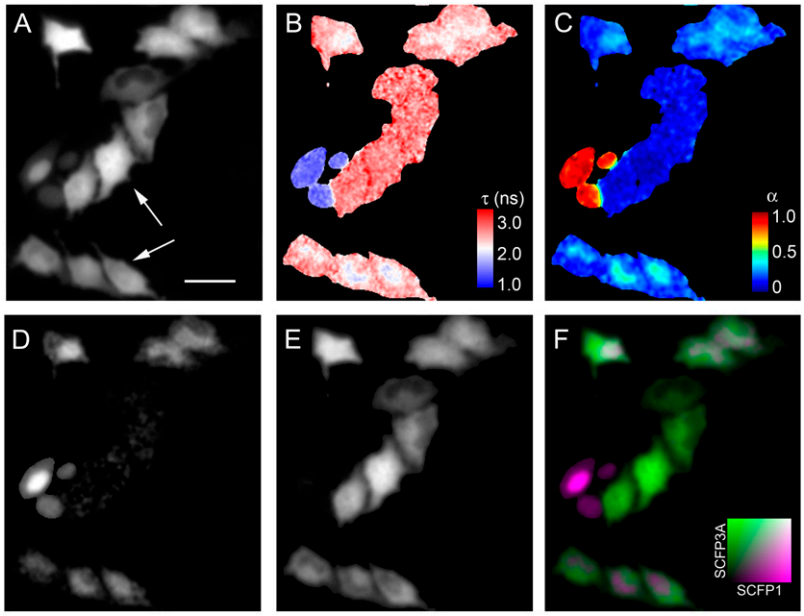

FIGURE 3 Lifetime unmixing of SCFP1 and SCFP3A in HeLa cells. (*A*) Fluorescence micrograph of cells expressing SCFP1-NLS and SCFP3A-NES or SCFP1-NLS alone. Arrows indicate cells that cannot be distinguished, based on the distribution of fluorescence. (*B*) Lifetime map based on τ'_φ. (*C*) Map of the fractional contribution of SCFP1 to the steady-state fluorescence. (*D* and *E*) Micrographs of the fractional molar distribution of SCFP1-NLS and SCFP3A-NES, respectively. (*F*) Overlay of *D* and *E*, with SCFP1-NLS indicated in purple and SCFP3A-NES indicated in green. Lifetime values used for unmixing: SCFP3A τ_φ = 2.47 ns, τ_m = 2.63 ns; SCFP1 τ_φ = 1.23 ns, τ_m = 1.40 ns. Scale bar = 50 μm.

CFPs within single living cells. Despite targeting the VFPs to different subcellular locations, cells expressing one or two fluorescent proteins could not be identified reliably based on the localization of fluorescence (Fig. 3 *A*, cells indicated by *arrows*). In contrast, based on the FLIM measurements cells expressing a single fluorescent protein were readily identified by a uniform high (SCFP3A-NES: $\tau_\varphi = 2.47$ ns, $\tau_m = 2.63$ ns) or low (SCFP1-NLS: $\tau_\varphi = 1.23$ ns, $\tau_m = 1.40$ ns) lifetime (Fig. 3 *B*). Cells coexpressing both CFP variants displayed a heterogeneous lifetime distribution, with a lower lifetime in the nucleus compared to the cytosol. These lifetime values and Eq. 9 were used to map the fractional distribution of SCFP1-NLS. In Fig. 3 *C*, the calculated α (τ'_φ), ranging from 0 to 1, is represented in pseudocolor. Cells expressing only SCFP1-NLS or SCFP3A-NES have values of $\alpha \approx 1$ and $\alpha \approx 0$, respectively. In cells coexpressing both fluorescent proteins, SCFP1-NLS fluorescence was enriched twofold more in the nucleus ($\alpha \approx 0.4$) than in the cytosol ($\alpha \approx 0.2$). The localization pattern for the two proteins was not mutually exclusive, especially in cells expressing high levels of fluorescent protein.

So far, we have quantified the fractional contribution to the steady-state fluorescence. For quantitative imaging, however, the fractional molar distribution of fluorescent probes is more relevant. Because SCFP1 and SCFP3A have identical excitation and emission spectra, their fluorescence is detected with equal efficiency. Therefore, the fractional contribution to the steady-state fluorescence can be converted to the fractional molar contribution upon dividing by the intrinsic brightness of the VFPs (Table 1). Due to the low *QY* of SCFP1, the fractional contribution to the steady-state fluorescence underestimated the true amount of SCFP1 by a factor 2.4. The unmixed molar distributions for SCFP1 and SCFP3A are shown in Fig. 3, *D* and *E*. The overlay of these two images (Fig. 3 *F*) shows that SCFP1-NLS was present mainly in the nucleus, whereas SCFP3A-NES was excluded from the nucleus.

Visualization of protein translocation by lifetime unmixing

VFP-based biosensors that report on the synthesis of second messengers are powerful tools for studying signal transduction in living cells. The PH domain of Grp1 binds specifically to PtdIns(3,4,5)P_3, an important second messenger, and a fluorescent protein fused to PH-Grp1 can be used as a biosensor for measuring PtdIns(3,4,5)P_3 synthesis (20). This biosensor translocates from the cytosol to the plasma membrane upon PtdIns(3,4,5)P_3 synthesis. The translocation is difficult to visualize in extremely flat cells, such as Swiss3T3 fibroblasts. We tested whether lifetime unmixing can be used to visualize PtdIns(3,4,5)P_3 production after stimulation of Swiss3T3 cells with PDGF.

From the fluorescence lifetime image, fibroblasts expressing SGFP2-NES-PHgrp1 and SGFP2(T65G) were identified by a higher fluorescence lifetime in the cytosol than in the nucleus (Fig. 4). Control cells expressing only SGFP2(T65G) displayed a homogeneous low lifetime. Estimation of the fractional contribution of SGFP2-NES-PHgrp1 to the steady-state fluorescence in cells expressing both GFP variants indicated that in the cytosol SGFP2-NES-PHgrp1 and SGFP2(T65G) were both present ($\alpha \approx 0.5$), whereas in the nucleus the concentration of SGFP2-NES-PHgrp1 was reduced ($\alpha \approx 0.25$) (Fig. 4 *C*).

Upon stimulation with PDGF, an increase in lifetime was observed at the edges of cells coexpressing SGFP2-NES-

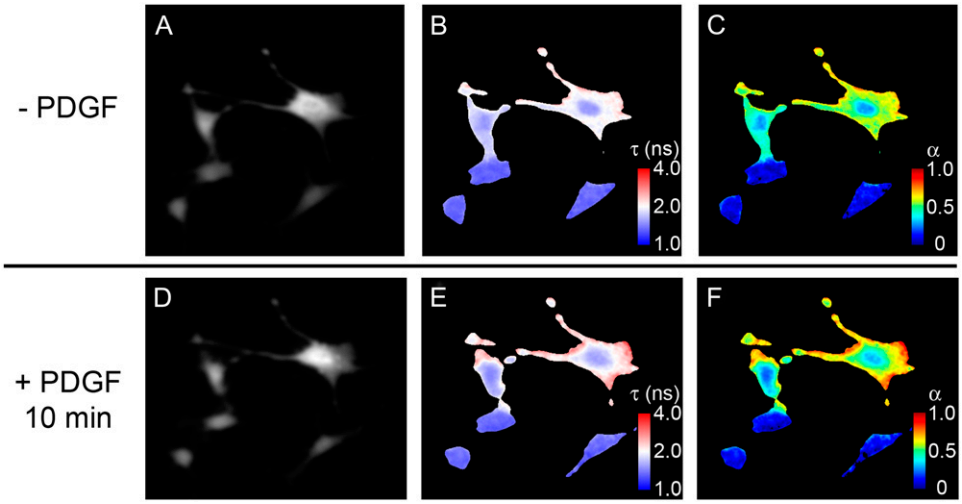

FIGURE 4 Translocation of a fluorescent biosensor for PtdIns(3,4,5)P_3 synthesis, visualized by lifetime unmixing. Cells were imaged before (*A–C*) and after (*D–F*) 10 min stimulation with PDGF. (*A* and *D*) Fluorescence micrographs of cells expressing SGFP2(T65G) and SGFP2-NES-PHgrp1, respectively. (*B* and *E*) Lifetime maps based on phase lifetime (τ'_φ). (*C* and *F*) Maps of the fractional contribution of SGFP2-NES-PHgrp1 to the total fluorescence. Lifetime values used for unmixing: SGFP2 $\tau_\varphi = 2.59$ ns, $\tau_m = 2.66$ ns; SGFP2(T65G) $\tau_\varphi = 1.25$ ns, $\tau_m = 1.30$ ns. Scale bar = 50 μm.

PHgrp1 and SGFP2(T65G) (Fig. 4 *E*). At these edges the fractional contribution of SGFP2-NES-PHgrp1 increased, whereas a decrease was observed in the cytosol surrounding the nucleus (Fig. 4 *F*). In the nucleus the fractional contribution of SGFP2-NES-PHgrp1 appeared to increase as well; however, this was more likely caused by accumulation of SGFP2-NES-PHgrp1 at the plasma membrane above and below the nucleus.

Lifetime unmixing was sensitive enough to visualize the translocation of a fluorescent fusion protein from the cytosol to the plasma membrane. This tends to be difficult when working with extremely flat cells, as was the case here. It was noted that during the live cell FLIM measurements photobleaching of SGFP2(T65G) was only ~5% and was similar to SGFP2.

Lifetime unmixing and multiparameter imaging

Lifetime unmixing of spectral identical compounds has great potential for multiparameter imaging because a single spectral channel can be used for resolving two species. To investigate the possibility of resolving four probes with only two spectral channels, we combined lifetime unmixing of SCFP3A and SCFP1 with FRET-FLIM measurements using the red-shifted donor/acceptor pair SYFP2 and mCherry. For this experiment mixed populations of HeLa cells were used,

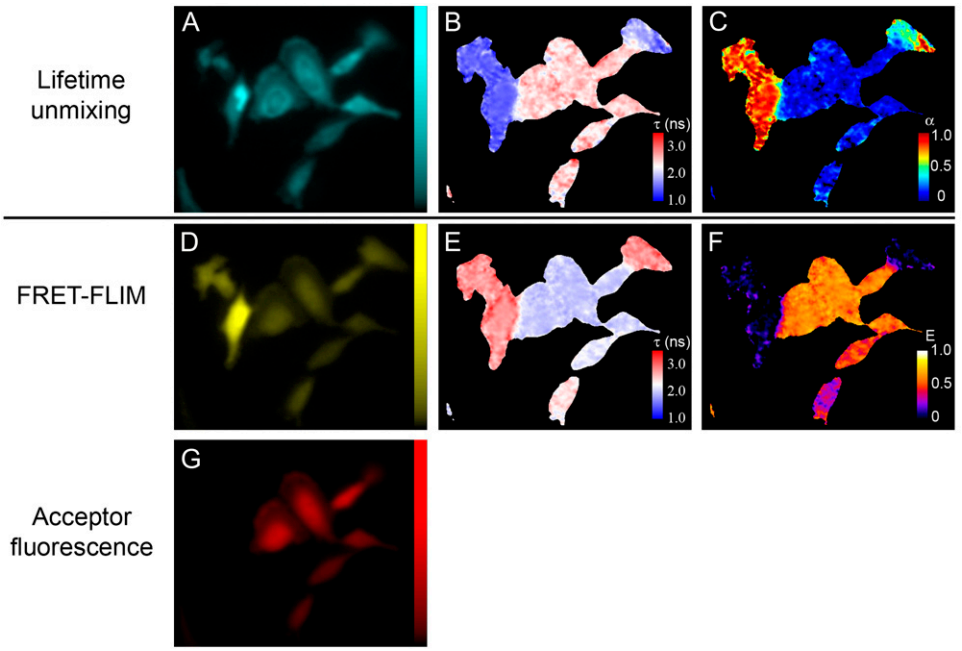

FIGURE 5 Multiparameter FLIM, combining lifetime unmixing with FRET-FLIM. (*A*, *D*, and *G*) Fluorescence micrographs of steady-state fluorescence of SCFP1/SCFP3A, SYFP2, and mCherry fluorescence, respectively. (*B*) Lifetime image based on SCFP fluorescence. (*C*) Fractional distribution of SCFP1. (*E*) Lifetime image based on SYFP2 fluorescence. (*F*) FRET efficiency map based on the fluorescence lifetime of SYFP2. Lifetime values used for unmixing: SCFP3A $\tau_\varphi = 2.47$ ns, $\tau_m = 2.63$ ns; SCFP1 $\tau_\varphi = 1.23$ ns, $\tau_m = 1.40$ ns. Scale bar = 30 μm.

expressing either SCFP1-NLS and SYFP2 or SCFP3A-NES and the tandem fusion mCherry-SYFP2. The CFP lifetime image clearly showed the presence of two cell populations with high (SCFP3A-NES) or low (SCFP1-NLS) fluorescence lifetimes, respectively (Fig. 5, *A* and *B*). Quantitative lifetime unmixing indicated that none of these cells was coexpressing both CFP variants (Fig. 5 *C*). All cells expressed SYFP2 in addition to CFP (Fig. 5 *D*); however, in cells containing SCFP3A-NES a reduced lifetime for SYFP2 was observed (Fig. 5 *E*). To verify that the reduced lifetime of SYFP2 was caused by FRET within the mCherry-SYFP2 dimer, the presence of mCherry was checked (Fig. 5 *G*). As expected, all cells with reduced SYFP2 lifetime expressed the mCherry-SYFP2 dimer. Based on the lifetimes observed for unfused SYFP2 ($\tau_D = 3.25$ ns) and SYFP2 within the tandem dimer ($\tau_{DA} = 2.20$ ns), the FRET efficiency for the mCherry-SYFP2 tandem dimer was estimated to be 32%, according to Eq. 13 (Fig. 5 *F*).

This experiment demonstrates the feasibility of imaging four different fluorescent probes with only two spectral channels. Furthermore the results are an example of combining quantitative imaging of noninteracting probes with FRET measurements of interacting probes.

DISCUSSION

In this study we have described a method for quantitatively unmixing the composition of binary mixtures of fluorophores with multiexponential fluorescence decays based on single-frequency FLIM data. Most existing methods depend on the availability of single-exponential decaying species, a condition that is hardly ever met in the complex interior of cells or when using complex chromophores such as VFPs. The only prerequisite for quantitative lifetime unmixing is that τ_φ and τ_m of the individual probes be known. In many studies τ_φ and τ_m of the individual probes are easily obtained, e.g., by using cells transfected with single probes.

Quantitative lifetime unmixing provides an alternative to the phasor plot approach. Both methods are able to unmix mixed fluorophores with multiexponential decays, and both methods determine the fractional composition based on the change in apparent phase shift and demodulation.

Lifetime unmixing yields two estimations of the fractional contribution, based on the apparent phase shift or demodulation, and both estimates should be the same. A deviation between the two estimates could indicate the presence of more than two fluorescent species in the sample or the presence of interacting fluorophores. Autofluorescence, for example, can give rise to an additional fluorescent species and should therefore be minimized. Representing the lifetime data in a phasor plot could help identify the presence of additional fluorescent species. Lifetime unmixing and the phasor plot both provide fast data analysis algorithms and are easily implemented together for a thorough analysis of FLIM data.

Relative concentrations of two probes or two fluorescent states of a single probe can also be obtained by intensity-based methods, for example, using fluorescence ratio-imaging (25–27) or a combination of spectral imaging and linear unmixing (28–30). However, obtaining quantitative fractional distributions of two probes from these intensity-based methods is difficult. This is because the fluorescence ratio or amplitude of the unmixed spectra is also dependent on the excitation light intensity, wavelength-dependent sensitivity of the detector(s) and filters used, chromatic aberrations, and (not in the case of spectral unmixing) potential cross talk between spectral channels (27,31). Obviously, when employing FLIM and lifetime unmixing with spectrally identical probes, such complications do not occur.

Applied to spectrally identical fluorophores, FLIM and lifetime unmixing allow quantitative determination of the fractional molar concentration for all pixels in an image if the intrinsic brightness of the fluorophores is known. The method is also applicable to mixtures of spectrally different fluorophores; however, to determine fractional molar concentration the detection efficiency of each fluorophore has to be known as well.

An important aspect when using VFPs is the pH dependence of the fluorescence. The absorbance of most VFPs is reduced at lower pH. When employing VFPs with different pK_as, acidification can alter the fractional contribution of each probe to the steady-state fluorescence. For SCFP3A and SCFP1 this is not a major issue, since their pK_a values are well below physiological range. For SGFP2 and SGFP2(T65G), however, the pK_a values are 5.9 and 6.7, respectively, and thus their fluorescence is more susceptible to changes in pH. Nevertheless, lifetime unmixing of neither SCFP1 and SCFP3A nor SGFP2 and SGFP2(T65G) appeared to be affected by pH over the range pH 6.5–8.0 (Data S1). Lifetime variations were observed between purified fluorescent proteins and fusion proteins expressed in mammalian cell, and similar effects have been reported by others (8,32). Hence, for accurate quantification of the fractional composition of binary mixtures by lifetime unmixing, it is important to measure τ_φ and τ_m of the pure compounds in a similar environment (e.g., cells) using the same fusion proteins.

Quantitative lifetime unmixing has potential for certain FRET studies, especially for FRET studies employing complex decaying VFPs as donor. The existence of only two states is prerequisite: a high FRET state and a low (or non-) FRET state. Furthermore, τ_φ and τ_m of the donor in both these states must be known from separate experiments. Under these conditions single-frequency lifetime unmixing can yield the fraction of donor in the high FRET state, irrespective of the complex fluorescence decay. FRET-based protein interaction studies can be addressed as a binary system of interacting (high FRET) and noninteracting (non-FRET) proteins. In many cases, unfortunately, τ_φ and τ_m in the interacting state are unknown and therefore lifetime unmixing cannot be applied to quantify the fraction of in-

teracting proteins. Analogously, for FRET sensors reporting on a conformational change, τ_φ and τ_m of the sensor in the high FRET and low FRET conformation must be known. Successful calibration of τ_φ and τ_m of these FRET states has been reported for several such FRET-based sensors, for example, the calcium sensor cameleon (33,34), a cAMP (adenosine 3′,5′-cyclic monophosphate) sensor (35), and a calpain protease sensor (36). Hence, for these sensors quantitative lifetime unmixing of the donor can provide the quantitative molar ratio of the biosensors in the FRET and non-FRET states (i.e., bound and free states) without the need for additional microscope-based correction factors. The bound/free concentrations ratio of the sensors can be transformed into molar concentrations of Ca^{2+} and cAMP using k_d values or in case of the calpain protease sensor, into the extent of proteolysis.

Quantitative analysis of FRET data by lifetime unmixing is based exclusively on the donor lifetime and therefore does not require the acceptor to be fluorescent. Hence, nonfluorescent but highly absorbing acceptors can be used. Such ''dark'' acceptors solve several complications common to FRET measurements. When using fluorescent acceptors, the spectral overlap necessary for efficient FRET is limited by the requirement for proper emission separation. Obviously, with dark acceptors this is not an issue. Hence, increased FRET efficiencies are possible by optimizing the spectral overlap between donor and acceptor. Furthermore, in the absence of acceptor fluorescence, a larger portion of the donor emission spectrum can be imaged, thereby improving the signal/noise ratio. Organic nonfluorescent acceptor dyes (37–39) as well as a dark YFP variant (40) for FRET are available. Furthermore, highly absorbing but nonfluorescent chromoproteins (41,42) offer high potential for additional VFP-based ''dark'' acceptors. Especially, conformational change FRET sensors employing a dark acceptor in combination with lifetime unmixing can provide quantitative measurements of the sensors in the high and low FRET states, using only one spectral channel. Application of dark acceptors in FRET experiments liberates a large part of the optical spectrum, thus allowing an increased number of FRET probes to be imaged in parallel.

In our opinion, quantitative lifetime unmixing of FLIM data will have a large impact on multiparameter imaging, also in view of the availability of spectral identical VFPs with distinct lifetimes. Multiparameter imaging aims at quantitative simultaneous imaging of as many interrelated biological processes as possible (43). We have demonstrated the possibility of detecting four VFP-based probes with two spectral detection channels. Additional different colored VFP lifetime variants will further increase the number of probes that can be imaged together. Other VFP lifetime variants have been developed, including variants of Aequorea victoria wild-type GFP and YFP (44,45). In addition, RFPs with distinct *QY*s (e.g., Plum and Katushka or mKate (46,47)) have recently become available that are expected to have distinct lifetimes. Hence, using CFP, YFP, and RFP variants, we expect that imaging six probes with three spectral detection channels will be feasible.

APPENDIX: THEORY OF FREQUENCY-DOMAIN FLIM

FLIM can be performed in different ways but is generally implemented using frequency-domain or time-domain approaches. FLIM requires that the excitation light be intensity modulated (frequency-domain) or pulsed (time-domain) and that the emitted fluorescence be measured time resolved. The theory of frequency-domain FLIM has been described extensively (17,48,49). In frequency-domain FLIM, the excitation light $E(t)$ is intensity modulated at high frequency (typically 10–100 MHz). As a result, the emitted fluorescence $F(t)$ is modulated at the same high frequency; but due to the noninstant fluorescence decay (i.e., the fluorescence lifetime), the emitted fluorescence will display a phase shift ($\Delta\varphi$) and demodulation ($M_F < M_E$) according to

$$E(t) = E_0(1 + M_E \sin\omega t) \tag{A1a}$$

$$F(t) = F_0(1 + M_F \sin(\omega t - \Delta\varphi)). \tag{A1b}$$

Here, E_0 is the average (steady-state) excitation intensity and F_0 is the average (steady-state) fluorescence intensity. The magnitude of the phase shift and demodulation depends on the fluorescence lifetime (τ) of the sample and on the angular frequency of modulation ($\omega = 2\pi f$), according to

$$\Delta\varphi = \tan^{-1}(\omega\tau), \tag{A2a}$$

$$\text{and} \quad M \equiv \frac{M_F}{M_E} = \frac{1}{\sqrt{1+\omega^2\tau^2}}. \tag{A2b}$$

Hence, it follows that two apparent fluorescence lifetimes τ_φ and τ_m can be defined from the observed phase shift and demodulation:

$$\tau_\varphi = \frac{1}{\omega}\tan(\Delta\varphi), \tag{A3a}$$

$$\text{and} \quad \tau_m = \frac{1}{\omega}\sqrt{\frac{1}{M^2} - 1}. \tag{A3b}$$

In the case of a multiexponential fluorescence decay, $\Delta\varphi$ and M are dependent on the individual lifetime components (τ_i) and their fractional contribution (to the steady-state fluorescence) (α_i), according to

$$\Delta\varphi = \tan^{-1}\left(\frac{X}{Y}\right), \tag{A4a}$$

$$\text{and} \quad M \equiv \frac{M_F}{M_E} = \sqrt{X^2 + Y^2} \tag{A4b}$$

with

$$\begin{cases} X = \sum_i \dfrac{\alpha_i\omega\tau_i}{1+\omega^2\tau_i^2} \\ Y = \sum_i \dfrac{\alpha_i}{1+\omega^2\tau_i^2} \end{cases}. \tag{A5a,b}$$

In Eqs. A5a,b α_i is a dimensionless constant with $\sum_i \alpha_i = 1$. For a fluorophore with monoexponential fluorescence decay, τ_φ and τ_m are equal. For samples with complex fluorescence decay, two apparent lifetimes are obtained, with $\tau_\varphi < \tau_m$ (3). Although quantitatively related to the lifetime components, these apparent lifetimes can be regarded as differently weighted average lifetimes of the complex fluorescence decay.

SUPPLEMENTARY MATERIAL

To view all of the supplemental files associated with this article, visit www.biophysj.org.

We thank D. W. Piston for critically reading the manuscript, R. Y. Tsien (mCherry) and C. Schultz (PHgrp) for providing plasmid DNA, and P. J. Verveer for providing and installing the global analysis software for single-frequency FLIM data analysis.

This work was supported by the European Union integrated project on Molecular Imaging (LSHG-CT-2003-503259).

REFERENCES

1. Dumas, D., and J. F. Stoltz. 2005. New tool to monitor membrane potential by FRET voltage sensitive dye (FRET-VSD) using spectral and fluorescence lifetime imaging microscopy (FLIM). Interest in cell engineering. *Clin. Hemorheol. Microcirc.* 33:293–302.
2. Lin, H. J., P. Herman, and J. R. Lakowicz. 2003. Fluorescence lifetime-resolved pH imaging of living cells. *Cytometry A.* 52:77–89.
3. Gadella, T. W. Jr., T. M. Jovin, and R. M. Clegg. 1993. Fluorescence lifetime imaging microscopy (FLIM): spatial resolution of microstructures on the nanosecond time scale. *Biophys. Chem.* 48:221–239.
4. Gadella, T. W. Jr., and T. M. Jovin. 1995. Oligomerization of epidermal growth factor receptors on A431 cells studied by time-resolved fluorescence imaging microscopy. A stereochemical model for tyrosine kinase receptor activation. *J. Cell Biol.* 129:1543–1558.
5. Wouters, F. S., P. I. Bastiaens, K. W. Wirtz, and T. M. Jovin. 1998. FRET microscopy demonstrates molecular association of non-specific lipid transfer protein (nsL-TP) with fatty acid oxidation enzymes in peroxisomes. *EMBO J.* 17:7179–7189.
6. Peyker, A., O. Rocks, and P. I. Bastiaens. 2005. Imaging activation of two Ras isoforms simultaneously in a single cell. *ChemBioChem.* 6:78–85.
7. Gadella, T. W. Jr., G. N. van der Krogt, and T. Bisseling. 1999. GFP-based FRET microscopy in living plant cells. *Trends Plant Sci.* 4:287–291.
8. Pepperkok, R., A. Squire, S. Geley, and P. I. Bastiaens. 1999. Simultaneous detection of multiple green fluorescent proteins in live cells by fluorescence lifetime imaging microscopy. *Curr. Biol.* 9:269–272.
9. Verveer, P. J., F. S. Wouters, A. R. Reynolds, and P. I. Bastiaens. 2000. Quantitative imaging of lateral ErbB1 receptor signal propagation in the plasma membrane. *Science.* 290:1567–1570.
10. Cubeddu, R., D. Comelli, C. D'Andrea, P. Taroni, and G. Valentini. 2002. Time-resolved fluorescence imaging in biology and medicine. *J. Phys. D Appl. Phys.* 35:R61–R76.
11. Squire, A., P. J. Verveer, and P. I. Bastiaens. 2000. Multiple frequency fluorescence lifetime imaging microscopy. *J. Microsc.* 197:136–149.
12. Verveer, P. J., and P. I. Bastiaens. 2003. Evaluation of global analysis algorithms for single frequency fluorescence lifetime imaging microscopy data. *J. Microsc.* 209:1–7.
13. Verveer, P. J., A. Squire, and P. I. Bastiaens. 2000. Global analysis of fluorescence lifetime imaging microscopy data. *Biophys. J.* 78:2127–2137.
14. Hanley, Q. S., and A. H. A. Clayton. 2005. AB-plot assisted determination of fluorophore mixtures in a fluorescence lifetime microscope using spectra or quenchers. *J. Microsc.* 218:62–67.
15. Redford, G. I., and R. M. Clegg. 2005. Polar plot representation for frequency-domain analysis of fluorescence lifetimes. *J. Fluoresc.* 15:805–815.
16. Digman, M. A., V. R. Caiolfa, M. Zamai, and E. Gratton. 2008. The phasor approach to fluorescence lifetime imaging analysis. *Biophys. J.* 94:L14–L16.
17. Weber, G. 1981. Resolution of the fluorescence lifetimes in a heterogeneous system by phase and modulation measurements. *J. Phys. Chem.* 85:949–953.
18. Kremers, G. J., J. Goedhart, D. J. van den Heuvel, H. C. Gerritsen, and T. W. Gadella Jr. 2007. Improved green and blue fluorescent proteins for expression in bacteria and mammalian cells. *Biochemistry.* 46:3775–3783.
19. Kremers, G. J., J. Goedhart, E. B. van Munster, and T. W. Gadella Jr. 2006. Cyan and yellow super fluorescent proteins with improved brightness, protein folding, and FRET Forster radius. *Biochemistry.* 45:6570–6580.
20. Gray, A., J. Van Der Kaay, and C. P. Downes. 1999. The pleckstrin homology domains of protein kinase B and GRP1 (general receptor for phosphoinositides-1) are sensitive and selective probes for the cellular detection of phosphatidylinositol 3,4-bisphosphate and/or phosphatidylinositol 3,4,5-trisphosphate in vivo. *Biochem. J.* 344:929–936.
21. Shaner, N. C., R. E. Campbell, P. A. Steinbach, B. N. Giepmans, A. E. Palmer, and R. Y. Tsien. 2004. Improved monomeric red, orange and yellow fluorescent proteins derived from Discosoma sp. red fluorescent protein. *Nat. Biotechnol.* 22:1567–1572.
22. van Munster, E. B., and T. W. Gadella Jr. 2004. phiFLIM: a new method to avoid aliasing in frequency-domain fluorescence lifetime imaging microscopy. *J. Microsc.* 213:29–38.
23. Boens, N., W. Qin, N. Basaric, J. Hofkens, M. Ameloot, J. Pouget, J. P. Lefevre, B. Valeur, E. Gratton, M. vandeVen, N. D. Silva Jr., Y. Engelborghs, K. Willaert, A. Sillen, G. Rumbles, D. Phillips, A. J. Visser, A. van Hoek, J. R. Lakowicz, H. Malak, I. Gryczynski, A. G. Szabo, D. T. Krajcarski, N. Tamai, and A. Miura. 2007. Fluorescence lifetime standards for time and frequency domain fluorescence spectroscopy. *Anal. Chem.* 79:2137–2149.
24. van Munster, E. B., and T. W. Gadella Jr. 2004. Suppression of photobleaching-induced artifacts in frequency-domain FLIM by permutation of the recording order. *Cytometry.* 58A:185–194.
25. Nagy, P., G. Vamosi, A. Bodnar, S. J. Lockett, and J. Szollosi. 1998. Intensity-based energy transfer measurements in digital imaging microscopy. *Eur. Biophys. J.* 27:377–389.
26. Gordon, G. W., G. Berry, X. H. Liang, B. Levine, and B. Herman. 1998. Quantitative fluorescence resonance energy transfer measurements using fluorescence microscopy. *Biophys. J.* 74:2702–2713.
27. van Rheenen, J., M. Langeslag, and K. Jalink. 2004. Correcting confocal acquisition to optimize imaging of fluorescence resonance energy transfer by sensitized emission. *Biophys. J.* 86:2517–2529.
28. Gadella, T. W. Jr., G. Vereb Jr., A. E. Hadri, H. Rohrig, J. Schmidt, M. John, J. Schell, and T. Bisseling. 1997. Microspectroscopic imaging of nodulation factor-binding sites on living Vicia sativa roots using a novel bioactive fluorescent nodulation factor. *Biophys. J.* 72:1986–1996.
29. Zimmermann, T., J. Rietdorf, and R. Pepperkok. 2003. Spectral imaging and its applications in live cell microscopy. *FEBS Lett.* 546:87–92.
30. Thaler, C., S. V. Koushik, P. S. Blank, and S. S. Vogel. 2005. Quantitative multiphoton spectral imaging and its use for measuring resonance energy transfer. *Biophys. J.* 89:2736–2749.
31. Berney, C., and G. Danuser. 2003. FRET or no FRET: a quantitative comparison. *Biophys. J.* 84:3992–4010.
32. Borst, J. W., M. A. Hink, A. van Hoek, and A. J. Visser. 2005. Effects of refractive index and viscosity on fluorescence and anisotropy decays of enhanced cyan and yellow fluorescent proteins. *J. Fluoresc.* 15:153–160.
33. Miyawaki, A., O. Griesbeck, R. Heim, and R. Y. Tsien. 1999. Dynamic and quantitative Ca2+ measurements using improved cameleons. *Proc. Natl. Acad. Sci. USA.* 96:2135–2140.
34. Van Munster, E. B., G. J. Kremers, M. J. Adjobo-Hermans, and T. W. Gadella Jr. 2005. Fluorescence resonance energy transfer (FRET) measurement by gradual acceptor photobleaching. *J. Microsc.* 218: 253–262.
35. Ponsioen, B., J. Zhao, J. Riedl, F. Zwartkruis, G. van der Krogt, M. Zaccolo, W. H. Moolenaar, J. L. Bos, and K. Jalink. 2004. Detecting cAMP-induced Epac activation by fluorescence resonance energy transfer: Epac as a novel cAMP indicator. *EMBO Rep.* 5:1176–1180.
36. Vanderklish, P. W., L. A. Krushel, B. H. Holst, J. A. Gally, K. L. Crossin, and G. M. Edelman. 2000. Marking synaptic activity in

dendritic spines with a calpain substrate exhibiting fluorescence resonance energy transfer. *Proc. Natl. Acad. Sci. USA.* 97:2253–2258.

37. Giordano, L., T. M. Jovin, M. Irie, and E. A. Jares-Erijman. 2002. Diheteroarylethenes as thermally stable photoswitchable acceptors in photochromic fluorescence resonance energy transfer (pcFRET). *J. Am. Chem. Soc.* 124:7481–7489.
38. Wu, D., and E. R. Edelman. 2004. Resonance energy transfer for assessing the molecular integrity of proteins for local delivery. *Biotechnol. Bioeng.* 85:406–412.
39. Chen, C. T., H. Wagner, and W. C. Still. 1998. Fluorescent, sequence-selective peptide detection by synthetic small molecules. *Science.* 279: 851–853.
40. Ganesan, S., S. M. Ameer-Beg, T. T. Ng, B. Vojnovic, and F. S. Wouters. 2006. A dark yellow fluorescent protein (YFP)-based resonance energy-accepting chromoprotein (REACh) for Forster resonance energy transfer with GFP. *Proc. Natl. Acad. Sci. USA.* 103:4089–4094.
41. Martynov, V. I., B. I. Maksimov, N. Y. Martynova, A. A. Pakhomov, N. G. Gurskaya, and S. A. Lukyanov. 2003. A purple-blue chromoprotein from Goniopora tenuidens belongs to the DsRed subfamily of GFP-like proteins. *J. Biol. Chem.* 278:46288–46292.
42. Gurskaya, N. G., A. F. Fradkov, A. Terskikh, M. V. Matz, Y. A. Labas, V. I. Martynov, Y. G. Yanushevich, K. A. Lukyanov, and S. A. Lukyanov. 2001. GFP-like chromoproteins as a source of far-red fluorescent proteins. *FEBS Lett.* 507:16–20.
43. Schultz, C., A. Schleifenbaum, J. Goedhart, and T. W. Gadella Jr. 2005. Multiparameter imaging for the analysis of intracellular signaling. *ChemBioChem.* 6:1323–1330.
44. Scruggs, A. W., C. L. Flores, R. Wachter, and N. W. Woodbury. 2005. Development and characterization of green fluorescent protein mutants with altered lifetimes. *Biochemistry.* 44:13377–13384.
45. Esposito, A., H. C. Gerritsen, and F. S. Wouters. 2005. Fluorescence lifetime heterogeneity resolution in the frequency domain by lifetime moments analysis. *Biophys. J.* 89:4286–4299.
46. Shcherbo, D., E. M. Merzlyak, T. V. Chepurnykh, A. F. Fradkov, G. V. Ermakova, E. A. Solovieva, K. A. Lukyanov, E. A. Bogdanova, A. G. Zaraisky, S. Lukyanov, and D. M. Chudakov. 2007. Bright far-red fluorescent protein for whole-body imaging. *Nat. Methods.* 4:741–746.
47. Wang, L., W. C. Jackson, P. A. Steinbach, and R. Y. Tsien. 2004. Evolution of new nonantibody proteins via iterative somatic hypermutation. *Proc. Natl. Acad. Sci. USA.* 101:16745–16749.
48. Clegg, R. M., and P. C. Scheider. 1996. Fluorescence lifetime-resolved imaging microscopy: a general description of lifetime-resolved imaging measurements. *In* Fluorescence Microscopy and Fluorescent Probes. J. Slavík, editor. Plenum Press, New York. 15–33.
49. Gadella, T. W. 1999. Fluorescence lifetime imaging microscopy (FLIM): instrumentation and applications. *In* Fluorescent and Luminescent Probes, 2nd ed. W. Mason, editor. Academic Press, London. 467–479.